An antibacterial Zn–MOF with hydrazinebenzoate linkers

An Antibacterial Zn–MOF with Hydrazinebenzoate Linkers

Jimmy Restrepo[1], Zakarias Serroukh[1], Javier Santiago[2], Sonia Aguado[2], Pilar Gómez-Sal[1,*], Marta E.G. Mosquera[1,*] and Roberto Rosal[1]

[1] Inorganic Chemistry Department. University of Alcalá, 28805, Alcalá de Henares, Madrid, Spain.
[2] Department of Chemical Engineering, University of Alcalá, 28805, Alcalá de Henares, Madrid, Spain.

* Corresponding authors: martaeg.mosquera@uah.es, pilar.gomez@uah.es

Abstract

A Zn-based metal–organic framework (MOF) with hydrazinebenzoate linkers was evaluated as antimicrobial material against the Gram-positive bacterium *Staphylococcus aureus*. The material inhibits bacterial growth and metabolic activity, with a half maximal effective concentration of about 20 mg L^{-1} material dispersed in the culture medium. The antimicrobial effect can be attributed to the release of the 4-hydrazinebenzoate linker, with a negligible contribution from the free metal. The material exhibits remarkable durability, and it enables the sustained release of the ligand over a period of several days.

Introduction

Healthcare-associated infections in hospitals cause significant economic consequences on healthcare systems, representing huge financial losses. Most of infections are produced by drug resistant or multidrug resistant Gram-negative bacteria such as *Escherichia coli*, *Klebsiella pneumonia*, and *Pseudomonas aeruginosa* as well as Gram-positive bacteria, for example *Staphylococcus aureus* [1].

Usually, bacteria contained in biofilms exhibit an increased tolerance against antimicrobial drugs; thus, in addition to exhibiting biocidal characteristics, antimicrobial materials have to avoid the growth of bacteria and its adhesion to surfaces. Traditionally, disinfection treatments use several chemical agents. However, they have the drawback of product breakdown and lack of long-term stability [2]. The design of new antibacterial materials is one of the most important challenges in the development of new strategies for the control of healthcare associated infections. The interest on antibacterial materials increases because of their potential to supply safety and quality to different environments [3].

Hybrid organic-inorganic and inorganic materials are well known as antimicrobials due to the release of metal ions. Among them, compounds containing silver are the most known because of their strong antibacterial activity and high stability [4]. However, silver is expensive and raises concern on its potentially harmful effects on our health and the environment. Zinc, on the contrary, is an inexpensive non-toxic d-block metal widely used as component of many drugs and cosmetics. Notably, it acts as a cicatrizing agent and skin moisturiser with antidandruff, astringent, anti-inflammatory and antibacterial properties [5].

Within hybrid organic-inorganic materials metal–organic frameworks (MOFs) constitute an important class [6]. These crystalline porous materials have large surface areas and tunable pore sizes that make them well suited for a variety of applications including gas storage, molecular sieving, sensors or heterogeneous catalysis [7]. MOFs are attractive materials since their structures can be designed at an atomic scale by an appropriate choice of metal and organic ligand. Compared with traditional chemical disinfectants, MOF antibacterial agents have many advantages in a wide antibacterial spectrum, long-term persistence, high effectiveness, and metal release control. However, so far few examples of MOFs with antibacterial activity have been reported, including Ag based MOFs [8] prepared with cobalt as metal [9] or based on copper [10]. Regarding to Zn based MOFs, Wang et al. prepared four different morphologies of zinc(II)-carboxylate coordination polymer particles and studied their antibacterial activities against *Bacillus subtilis*, *S. aureus*, *Salmonella enteritidis*, *E. coli*, *Proteus vulgaris* and *P. aeruginosa* by determining the minimum inhibitory concentrations [11]. More recently, Tamames et al. formulated a biocompatible and bioactive BioMIL-5, synthesized from a Zn^{2+} salt and azelaic acid, showing biocide properties against *S. aureus* and *Staphylococcus epidermidis* [12].

In this paper we described a Zn-based MOF and its antibacterial activity. The linker of choice is 4-hydrazinebenzoate. The coordination chemistry of this molecule has been hardly explored and very few compounds have been described [13]. However, it is a molecule of biological interest [14] and in fact is used for the preparation of Deferasirox, an orally active iron chelating agent for the treatment of iron overloads [15]. In order to assess the antimicrobial efficiency of the MOF, a strain of the Gram-positive bacterium *S. aureus* was used. It is a bacterium responsible for nosocomial infections with frequent resistance to antibiotics, has been associated to foodborne disease outbreaks and is a leading cause of hospital acquired and health care associated infections. As well *S. aureus* is ordinarily used for testing the antibacterial activity of engineered surfaces (ISO 22196).

Results and Discussion

The framework $\{[Zn(\mu\text{-}4\text{-}hzba)_2]_2 \cdot 4(H_2O)\}_n$ (1) was prepared under biological compatible conditions using non toxic solvents. As such, 4-hydrazinebenzoic acid was dissolved in EtOH and an aqueous solution of $Zn(OAc)_2.nH_2O$ (Scheme 1) was added to this solution. The homogeneous mixture was heated at 110°C for 24 hours under hydrothermal conditions, from the mixture white-yellow crystals were isolated. The crystals had enough quality for a Single Crystal X-ray diffraction study which allowed us for the elucidation of its structure in the solid state.

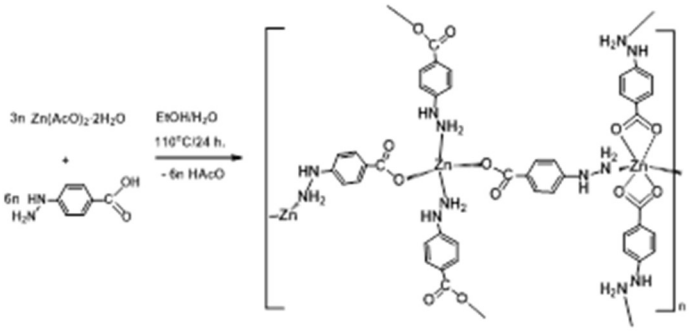

Scheme 1. Synthesis of $\{[Zn(\mu\text{-}4\text{-}hzba)_2]_2 \cdot 4(H_2O)\}_n$ (**1**).

In the solid structure of compound 1, two different environments are observed for the Zn atoms (Figure 1). In one case, the Zn center is tetracoordinated with a tetrahedral environment while the second one is hexacoordinated with an octahedral symmetry. Each tetrahedral nucleus is connected to four octahedral Zn by four 4-hzba linkers and vice versa. Both types of Zn atoms are bonded to two 4-hydrazinebenzoates by the NH_2 group and to two other ligands by the carboxylate moiety.

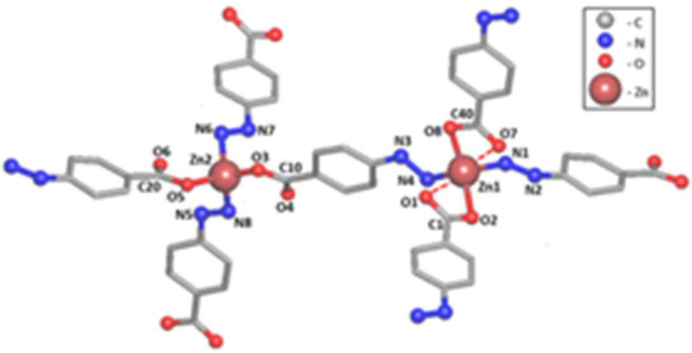

Figure 1. Crystal structure of $\{[Zn(\mu\text{-}4\text{-}hzba)_2]_2 \cdot 4(H_2O)\}_n$ (**1**)

The difference in the coordination environment relays in the way the carboxilate group is bonded: as a chelate for the octahedral Zn center and monodentated for the other Zn atom. The shortest Zn-O distances in the molecule corresponds to the monocoordinated carboxylate groups (table 1).

The metal atoms are connected by bridging 4-hydrazinebenzoate ligands creating an extended network. The network present big pores (18.58 by 14.83 Å) and interpenetration occurs. As such, five interpenetrated 3D networks are present in compound **1**, this feature hampers porosity in **1**, however it is not a necessary characteristic for this particular application. In figure 2 a view of the entanglement is shown. The different colours, red, green, yellow, blue and purple have been assigned to each network for clarity. In the pores water guest molecules are placed. In an analysis of the simplified network, it can be described as uninodal 4-connected. The topology of the network is dia-Diamond, 4/6/c1, sqc6; with point symbol 6^6.

Table 1. Selected distances for compound **1**

Bond length (Å)			
Zn(1)-O(2)	2.053(10)	Zn(2)-N(6)	2.041(10)
Zn(1)-O(8)	2.070(9)	Zn(2)-N(8)	2.137(17)
Zn(1)-O(1)	2.346(12)	N(1)-N(2)	1.420(16)
Zn(1)-O(7)	2.367(10)	N(5)-N(6)	1.411(15)
Zn(2)-O(5)	1.935(10)	N(3)-N(4)	1.393(19)
Zn(2)-O(3)	1.942(12)	N(8)-N(7)	1.27(2)
Zn(1)-N(2)#1	2.114(12)	N(4)-Zn(1)#3	2.130(14)
Zn(1)-N(4)#2	2.130(14)	N(2)-Zn(1)#4	2.114(12)

Symmetry transformations used to generate equivalent atoms: #1 x-1,y+2,z #2 x-2,y,z+1 #3 x+2,y,z-1 #4 x+1,y-2,z

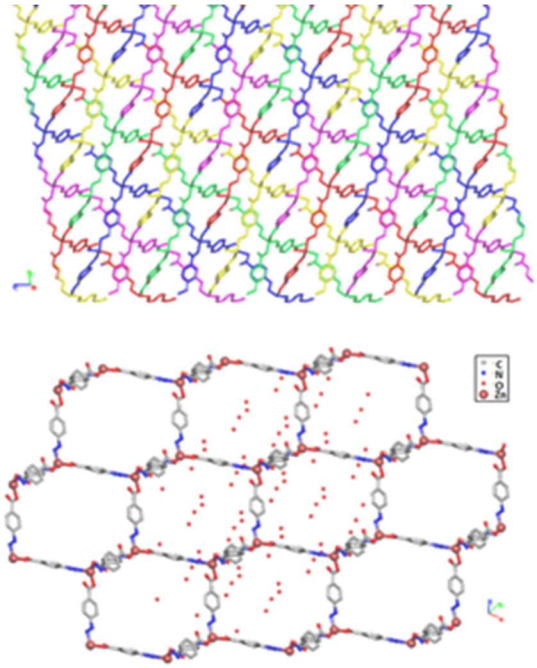

Figure 2. 3D network {[Zn(μ-4-hzba)$_2$]$_2$·4(H$_2$O)} along *a* (Top). One of the five 3D networks (Bottom). Hydrogen atoms and non-coordinated water have been omitted for clarity.

The thermal analysis shows a reduction of 10 % in weight up to 300°C, probably due to the loss of the uncoordinated water molecules present in the structure. Above this temperature the rapid decomposition of the material is observed as a consequence of the ligand loss (see SI).

In the IR spectrum the characteristic bands for the O-H, N-H, OCO, C-N, N-N, C=C y C-H (aromatic and sp^3), are observed. In this compound an interesting parameter is the Δν value for the symmetric and unsymmetric streching bands for the group OCO and to compare it with the value for the free ligand. It has been experimentally observed that $\Delta\nu_{chelate} < \Delta\nu_{bridge} < \Delta\nu_{ligand} < \Delta\nu_{monodentated}$ [16]. In **1**, two bands for the OCO asymmetric streching at 1674 cm-1 and 1602 cm-1, and one symmetric one at 1390 cm^{-1} are observed. With these values two Δν are obtained: 284 cm^{-1} that can be assigned to the monodentated coordination of the carboxylate group and Δν: 212 cm^{-1} that corresponds to the chelate coordinated, since Δν for the uncoordinated ligand is 247 cm^{-1}., in accordance with structure observed were both coordination modes, monodentated and chelate are present in the compound.

The antimicrobial activity of {[Zn(μ-4-hzba)$_2$]$_2$·4(H$_2$O)}$_n$ (**1**) and the ligand precursor, 4-hydrazinebenzoic acid, was tested in solid form by placing 1 mg of each material in agar plates at 36°C and incubating them for 24 h after inoculation with 200 μL of *S. aureus* suspension containing 5·10^7 colony-forming units (CFU)·mL^{-1}. A lawn of bacteria forms on the agar surface except in the areas in which compound **1** inhibited microbial growth. The results are shown in Figure 3 in which the numbers refer to replicates of the same material and "L" to the ligand. As shown in the picture in all cases inhibition was observed. The average inhibition diameter for all compound **1** samples was 14.6 ± 3.1 mm. The outer diameter for the inhibition disk of the ligand precursor was 11.5 ± 2.2 mm. It is interesting to note that the assay conditions represent a stringent scenario for the testing of an antimicrobial compound as it is carried out during the exponential growth phase of the microorganism in its culture media and at their optimum growth temperature.

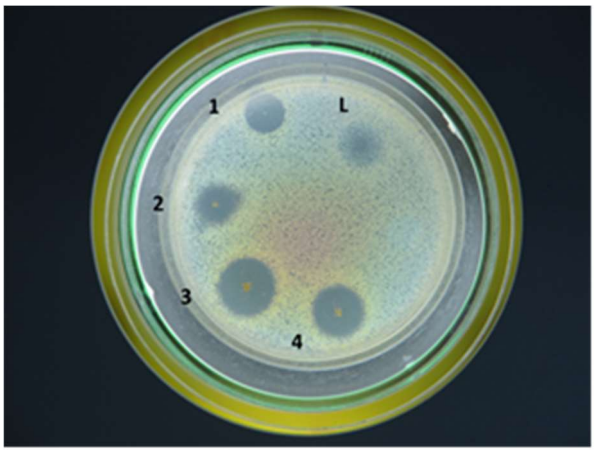

Figure 3. Inhibition areas for compound **1** (four different tests) and the ligand.

In order to clarify the toxic effect of compound **1**, inhibition curves were prepared by dispersing compound **1** in the liquid culture media of *S. aureus*. The dispersion was sonicated and kept under stirring the time necessary for a complete release of the metal and ligand present in compound **1**. The purpose was to compare the effects of the fragments on the bacteria. For it, the amount of metal in solution was determined using the method of 4-pyridylazoresocinol as explained below (Experimental Section). The amount of metal in solution was > 90% in a suspension that was sonicated, filtered and analysed 2 h after placing compound **1** in contact with water or culture medium. The results are shown in Figure 4 for the inhibition of the metabolic bacterial activity by means of the FDA method, which measures metabolically active cells (the results expressed as inhibition of colony forming units are shown in Supporting Information). The inhibition curves of compound **1** and the ligand precursor were essentially coincident indicating that the antimicrobial activity of compound **1** run in parallel with that of 4-hydrazinebenzoate. Median effect values (EC$_{50}$) were computed using the ICp software freely available from EPA statistical computer programs [17]. ICp approach

uses a nonparametric monotonic regression that does not depend on any particular model allowing point estimates and confidence intervals without any mechanistic assumption. The EC_{50} values for the metabolic impairment were 22.3 ± 4.8 mg·L^{-1} and 28.0 ± 5.2 mg·L^{-1} for the ligand and compound **1** respectively. Considering the capacity of forming viable colonies (in S.I.), the EC_{50} values were 24.2 ± 3.4 mg·L^{-1} and 27.5 ± 4.4 mg·L^{-1} for compound **1** and the ligand precursor. Taking into account the stoichiometric amount of 4-hydrazinebenzoate in compound **1**, the ligand explains all 90% of the loss capacity of forming new colonies and all of the metabolic damage. The higher degree of colony forming reduction with respect to the metabolic activity for bacteria exposed to a toxicant is commonly observed in disinfection processes and is related to the presence of viable but non-culturable bacteria, which are those that remain metabolically active, but fail to divide and do not have the capacity to form viable colonies [18]. For the lower exposures, a negative inhibition was observed for FDA metabolic activity, which was most probably due to the stimulating effect of low concentrations of zinc.

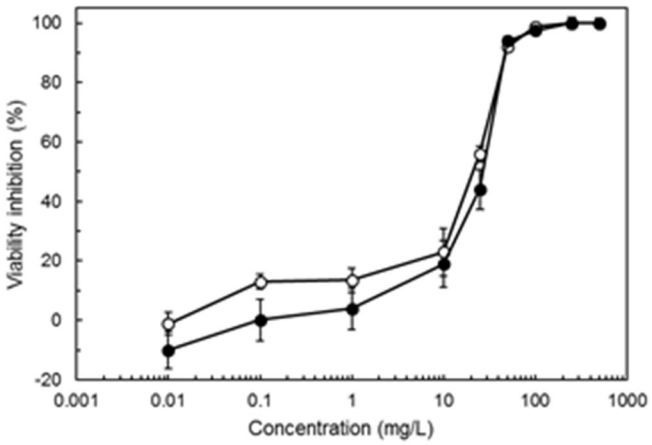

Figure 4. Viability (FDA) inhibition of *S. aureus* cells in contact with {[Zn(μ-4-hzba)$_2$]$_2$·4(H$_2$O)}$_n$ (**1**) (filled dots) and the ligand (empty dots).

Zinc is an essential metal with relatively low toxicity towards *S. aureus*. Its low toxicity is due to its role as an important cofactor for many enzymes. Zinc ions can show toxic effects at high concentrations, but the minimum inhibitory concentration for zinc ions for *S. aureus* was reported in the 2-20 mM range (65-131 mg/L) [19]. Excess zinc has significant toxicity to bacteria at high concentrations either in free form or as zinc-releasing materials [20]. The exact mechanism of zinc toxicity has not been fully explained, although the irreversible binding to certain surface adhesins may explain the bacterial susceptibility to Zn^{2+} [21]. Most bacterial strains are known to develop considerable resistance against certain metal ions. The mechanisms for this biological resistance have been attributed to the modification in protein expression encoded by plasmid-mediated resistance genes, which is triggered by the exposition to high concentration of metals [22]. The role of zinc as essential micronutrient for bacteria, which forced bacteria to develop metal acquisition and efflux systems able to cope with scarcity and excess of metal ions, explains their tolerance to high concentrations of zinc [23].

The release of ligand from compound **1** was studied in water solution and on agar plates using the same medium used for recording the data shown in Figure 4. In pure water at 20 °C, the rate of release was 0.04 mg of 4-hydrazinebenzoate/(mg compound **1** h). This represented 85% ligand release after 48 h. Upon tracking the metal in solution, the amount of zinc in solution represented 76 ± 4 % of the initial metal content. On agar plates, the rate of ligand release is shown in Figure 5. The stability of compound **1** was significantly higher in these conditions, allowing a 78% of compound **1** still forming the solid framework after 96 h at 20 °C. The data for the ligand shown in Figure 5 reflected the fact that 4-hydrazinebenzoate quickly dispersed on the surface of nutrient agar so that after a few hours it was not possible to identify any remaining solid form the material deposited on it and the percentage of ligand recovered from the agar plate approached 100%.

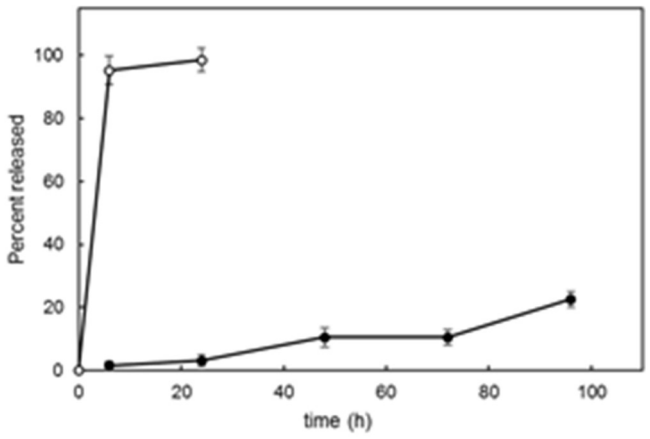

Figure 5. Release of ligand recorded for {[Zn(μ-4-hzba)$_2$]$_2$·4(H$_2$O)}$_n$ (**1**) on agar plates (filled dots) and the result of the same experiment for the ligand alone (empty dots).

The release of the ligand was also studied in solution by NMR spectroscopy. For it, compound **1** was placed in the liquid culture medium for bacteria and kept at 36 °C. Then a ^{1}H NMR study was performed after 6 hours and on the course of several days. As shown in figure 6, after few hours the bands corresponding to the

ligand were observed in the characteristic area of the aromatic protons proving the ligand release. After a week the evolution to generate other species in the media was clearly evidenced in the spectra since more bands appeared (figure 6 top). In order to compare the same experiments were performed just with the ligand precursor in the culture liquid. In this case the evolution was faster than for the compound **1** and the final products formed are different as signals at different shift values are observed. Although in the reaction media it is difficult to identify the products, the formation of a mixture of species with substituted aromatic rings is clear.

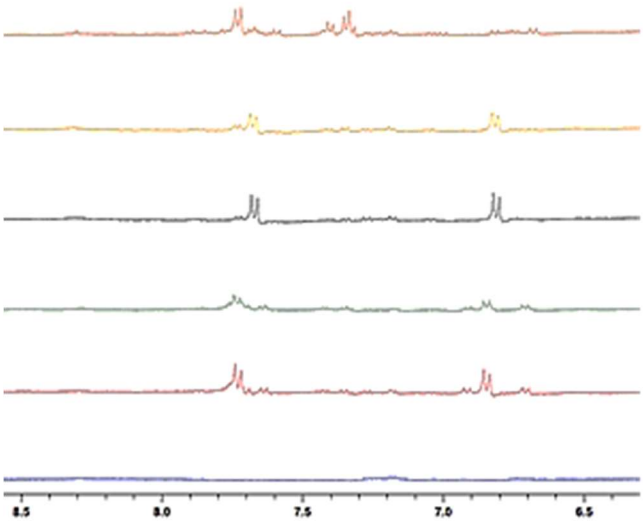

Figure 6. ^{1}H NMR spectra in D_2O/H_2O from bottom to top: the culture liquid, the ligand after six hours at 36°C in the culture liquid, the ligand after two days at 36°C in the culture liquid, compound **1** after six hours at 36°C in the culture liquid, after two days and after six days.

The data indicated that compound 1 allows for a slower and more controlled release of a species with antibacterial properties, ensuring a longer antibacterial effect without releasing other substances to the medium different from zinc ions.

Conclusions

The Zn-based MOF $\{[Zn(\mu\text{-}4\text{-}hzba)_2]_2 \cdot 4(H_2O)\}_n$ prepared with 4-hydrazinebenzoic acid displays significant antibacterial behaviour inhibiting the growth and metabolic activity of the Gram-positive bacterium *S. aureus*. The impairment can be ascribed to the release of the ligand. The material exhibits remarkable antibacterial durability, due to the controlled release of the ligand that can be an important feature in order to develop materials that can keep the antibacterial properties for longer periods of time. The zinc released with the ligand does not influence the antibacterial activity of the material, but its stoichiometry ensures a controlled biological effect of the ligand.

Experimental section

General procedure. All reagents and solvents were commercially available and used as received without further purification.

Synthesis of compound 1. 0.076 g (0.5 mmol) of 4-hydrazinobenzoic acid (4-hzbaH) and 0.111 g (0.5 mmol) of $Zn(AcO)_2 \cdot 2H_2O$ are placed in a Teflon-lined Parr reactor. To this mixture 6 mL de H_2O Milli-Q and 5mL of EtOH 99.5% were added. The reaction is heated at 110°C for 24 hours.

Then the reactor is left to cool down to room temperature. Yellow crystals can be isolated for the mixture formed. Yield (based on Zn): 0.062 g (0.077 mol), 31.02 %. Elemental Analysis $C_{14}H_{14}N_4O_6Zn \cdot 4H_2O$: Calc: C, 41.44; H, 4.78; N, 12.08. Exp: C, 40.65; H, 4.45; N, 12.26. IR (cm^{-1}, KBr): □(OCO) 1674 (m), 1603 (s) and 1390 (s); □(N-H) 3350 (m) and 1552 (s); ν(O-H) 3201 (s, br); ν(C-N) 1256.59 (vs); ν(C-$H_{aromatic}$) 2964 (w) and 779 (s). 1180 ν (N-N)

Single Crystal X-ray study for 1. Details of the X-ray experiment, data reduction, and final structure refinement calculations are summarized in Table S2. Suitable single crystals of **1** for the X-ray diffraction study were selected. Data collection was performed at 200(2) K, with the crystals covered with perfluorinated ether oil. The crystals were mounted on a Bruker-Nonius Kappa CCD single crystal diffractometer equipped with a graphite-monochromated Mo-Kα radiation (λ = 0.71073 Å). Data were measured with exposure times of 360 s per frame (3 sets; 159 frames; phi/omega scans; 2.0° scan-width). Raw data were corrected for Lorenz and polarization effects. Multiscan [24] absorption correction procedures were applied to the data. The structures were solved, using the WINGX package [25], by direct methods (SHELXS-97) and refined using full-matrix least-squares against F^2 (SHELXL-97) [26]. All non-hydrogen atoms were anisotropically refined, with the exception of O8, N6, C20, C30 and hydrogen atoms were geometrically placed and left riding on their parent atoms. In the structure four oxygen atoms from water solvent appear, but the corresponding hydrogen atoms were not found. Crystallographic data (excluding structure factors) for the structure reported in this paper have been deposited with the Cambridge Crystallographic Data Centre as supplementary publication no. CCDC-1484492 [**1**]. Copies of the data can be obtained free of charge on

application to CCDC, 12 Union Road, Cambridge CB2 1EZ, UK (fax: (+44)1223-336-033; e-mail: deposit@ccdc.cam.ac.uk).

Microbial assays. The Gram-positive *S. aureus* (CETC 240) bacterial strain was used to assess the antibacterial activity of MOF and ligand. Bacteria were kept at −80°C in glycerol (20% v/v) until use and its reactivation was performed in nutrient broth (10 g L^{-1} peptone, 5 g L^{-1} sodium chloride, 5 g L^{-1} meat extract, pH 7.0 ± 0.1) controlled by measuring optical density (OD) at 600 nm. Agar plates were prepared by dissolving 2.5 g L^{-1} yeast extract, 5.0 g L^{-1} tryptone, 1.0 g L^{-1} glucose and 15.0 g L^{-1} agar powder in deionized water. The mixture was heated under stirring until the agar dissolved, pH adjusted to 7.0 ± 0.1 with sodium hydroxide or hydrochloric acid and sterilized by autoclaving.

The biocidal effect of MOF and ligand were studied by means of the diffusion method. 200 µL of the bacterial suspension containing $5 \cdot 10^7$ colony-forming units (CFU)/mL were spread on agar plates. After plates were air dried, 1 mg of material was disposed directly onto agar surface and the plates, together with controls and sterile Petri dishes, after which the plates were incubated at 36°C for 24 h. Diameters corresponding to growth inhibition area were determined by digital image analysis with the open source program Image J. Three replicates have been performed.

The antimicrobial effect of the ligand was assessed by exposing liquid cultures of *S. aureus*. A dilution series was prepared from a stock of 500 mg·L^{-1} of each material dispersed using an ultrasound bath for 15 min. 2 mL of each dilution was placed into the wells of sterile 24-well plates together with the prescribed bacterial inoculum to achieve an initial concentration of 10^6 cells·mL^{-1}. Plates were incubated at 36 ± 1 °C for 20 h. Then, an aliquot of cultures was transferred to a sterile 96 well microtiter plates and diluted in phosphate-buffered saline (PBS) medium following a 10-fold series. 10 µL of each PBS dilution were spot-plated on agar Petri dishes. After incubation at 36°C for 24h, colony forming units (CFU) were scored with a CL-1110 counting instrument (Acequilabs, Spain). We considered at least three replicates of at least two serial dilutions for viable cell estimation.

The biocidal activity was also studied by assessing cell viability with fluorescein diacetate (FDA), a non-fluorescent compound which is transformed to the green fluorescent compound fluorescein when contacting active esterases in functional cells. 5 µL of FDA (0.02 % w/w in DMSO) were added to 195 µL of culture in 96-well black-sided microtiter and incubated for 20 h and incubated at 25°C. The fluorescein fluorescent was measured with a fluorimeter (ThermoScientific™ FL, Ascent) using an excitation wavelength of 485 nm and emission wavelength of 528 nm.

Release of metal. Metal concentration was determined using the 4- pyridylazoresocinol (PAR), whose absorbance at 500 nm increases when it chelates Zn to generate Zn-PAR complex [27]. Aliquots at prescribed times were withdrawn and filtered through 0.22 µm. 1 mL of sample was mixed with PAR solution (300 mM) prepared in ultrapure water and 1 ml phosphate buffered saline (100 mM, pH 7). The absorbance of the mixture was measured at 500 nm using a Shimadzu UV Spectrophotometer UV-1800.

Release of ligand. The release of ligand was studied in water and on agar plates. In water, a weighted amount of material was suspended in water for a prescribed time after which, the solid was removed and the absorbance of the liquid recorded at 264 nm using a Shimadzu UV Spectrophotometer UV-1800. In another series of runs, 2 mg of the material, accurately weighted, were deposited in the middle of agar plates and kept at 20 °C for 6, 24, 48, 72 and 96 h. After the prescribed time, the remaining solid was carefully scrapped out of the agar and the whole content of the Petri was dissolved in hot water. The solution was allowed to cool to separate the insoluble solid agar and filtered using 0.45 µm glass fibre filters. The amount of ligand released was recorded in the liquid using the same UV spectrophotometer at 264 nm.

Solution ^{1}H NMR spectra were recorded at 400.13 MHz on a Bruker AV400 spectrometer using D_2O as solvent. ^{1}H chemical shifts are given relative to TMS (δ = 0 ppm) and were measured from the solvent resonances. In order to prepare the sample, 0.1 ml of D_2O was added to 0.3 ml of the mixture containing the cultive media and the compound.

Acknowledgements

Financial support for this work was provided by the FP7-ERA-Net Susfood, 2014/00153/001, the Spanish Ministry of Economy and Competitiveness, CTM2013-45775 and CTQ2014-58270-R, the Dirección General de Universidades e Investigación de la Comunidad de Madrid, Research Network S2013/MAE-2716, the Factoría de Cristalización-Consolider–Ingenio (CSD2006-00015) and the Alcalá University, Spain (CCG10-UAH/PPQ-5925).

Keywords: MOFs • Zn • Antibacterial • *S. aureus*

References

[1] S. S. Jean, P. R. Hsueh, W. S. Lee, H. T. Chang, M. Y. Chou, I. S. Chen, J. H. Wang, C. F. Lin, J. M. Shyr, W. C. Ko, J. J. Wu, Y. C. Liu, W. K. Huang, L. J. Teng, C. Y. Liu, *Eur. J. Clin. Microbiol. Infect. Dis.* **2010**, *29*, 471-475.

[2] R. A. Minear, G. L. Amy, in *Water disinfection and natural organic matter: Characterization and control* (Eds.: R. A. Minear, G. L. Amy), American Chemical Society, Washington, D.C., **1996**, p. Ch. 1.

[3] E.-R. Kenawy, S. D. Worley, R. Broughton, *Biomacromolecules* **2007**, *8*, 1359-1384.

[4] a) K. Belser, T. V. Slenters, C. Pfumbidzai, G. Upert, L. Mirolo, K. M. Fromm, H. Wennemers, *Angew. Chem. Int. Ed.* **2009**, *48*, 3661-3664; b) K. M. Fromm, *Coord. Chem. Rev.* **2008**, *252*, 856-885; c) K. M. Hindi, T. J. Siciliano, S. Durmus, M. J. Panzner, D. A. Medvetz, D. V. Reddy, L. A. Hogue, C. E. Hovis, J. K. Hilliard, R. J. Mallet, C. A. Tessier, C. L. Cannon, W. J. Youngs, *J. Med. Chem.* **2008**, *51*, 1577-1583; d) A. Kumar, P. K. Vemula, P. M. Ajayan, G. John, *Nat. Mater.* **2008**, *7*, 236-241; e) T. V. Slenters, J. L. Sague, P. S. Brunetto, S. Zuber, A. Fleury, L. Mirolo, A. Y. Robin, M. Meuwly, O. Gordon, R. Landmann, A. U. Daniels, K. M. Fromm, *Materials* **2010**, *3*, 3407-3429.

[5] J. R. Schwartz, R. G. Marsh, Z. D. Draelos, *Dermatol. Surg.* **2005**, *31*, 837-847.

[6] a) G. Ferey, *Chem. Soc. Rev.* **2008**, *37*, 191-214; b) S. Kitagawa, R. Kitaura, S. Noro, *Angew. Chem. Int. Ed.* **2004**, *43*, 2334-2375; c) O. M. Yaghi, M. O'Keeffe, N. W. Ockwig, H. K. Chae, M. Eddaoudi, J. Kim, *Nature* **2003**, *423*, 705-714.

[7] a) L. Alaerts, C. Kirschhock, M. Maes, M. van der Veen, V. Finsy, A. Depla, J. Martens, G. Baron, P. Jacobs, J. Denayer, D. De Vos, *Angew. Chem. Int. Ed.* **2007**, *46*, 4293-4297; b) M. Eddaoudi, J. Kim, N. Rosi, D. Vodak, J. Wachter, M. O'Keefe, O. M. Yaghi, *Science* **2002**, *295*, 469-472; c) D. Farrusseng, S. Aguado, C. Pinel, *Angew. Chem. Int. Ed.* **2009**, *48*, 7502-7513; d) B. Harbuzaru, A. Corma, F. Rey, P. Atienzar, J. Jordá, H. García, D. Ananias, L. Carlos, R. Rocha, *Angew. Chem. Int. Ed.* **2008**, *47*, 1080-1083; e) P. L. Llewellyn, S. Bourrelly, C. Serre, A. Vimont, M. Daturi, L. Hamon, G. De Weireld, J.-S. Chang, D.-Y. Hong, Y. Kyu Hwang, S. Hwa Jhung, G. Ferey, *Langmuir* **2008**, *24*, 7245-7250; f) T. Loiseau, L. Lecroq, C. Volkringer, J. Marrot, G. Ferey, M. Haouas, F. Taulelle, S. Bourrelly, P. L. Llewellyn, M. Latroche, *J. Am. Chem. Soc.* **2006**, *128*, 10223-10230.

[8] a) M. Berchel, T. Le Gall, C. Denis, S. Le Hir, F. Quentel, C. Elleouet, T. Montier, J. M. Rueff, J. Y. Salauen, J. P. Haelters, G. B. Hix, P. Lehn, P. A. Jaffres, *New J. Chem.* **2011**, *35*, 1000-1003; b) Y. Liu, X. Xu, Q. Xia, G. Yuan, Q. He, Y. Cui, *Chem. Comm.* **2010**, *46*, 2608-2610; c) X. Lu, J. Ye, D. Zhang, R. Xie, R. F. Bogale, Y. Sun, L. Zhao, Q. Zhao, G. Ning, *J. Inorg. Biochem.* **2014**, *138*, 114-121.

[9] a) S. Aguado, J. Quiros, J. Canivet, D. Farrusseng, K. Boltes, R. Rosal, *Chemosphere* **2014**, *113*, 188-192; b) W. Zhuang, D. Yuan, J.-R. Li, Z. Luo, H.-C. Zhou, S. Bashir, J. Liu, *Adv. Healthcare Mater.* **2012**, *1*, 225-238.

[10] a) H. S. Rodriguez, J. P. Hinestroza, C. Ochoa-Puentes, C. A. Sierra, C. Y. Soto, *J. Appl. Polym. Sci.* **2014**, *131*; b) C. Wang, X. Qian, X. An, *Cellulose* **2015**, *22*, 3789-3797.

[11] K. Wang, Y. Yin, C. Li, Z. Geng, Z. Wang, *CrystEngComm* **2011**, *13*, 6231-6236.

[12] C. Tamames-Tabar, E. Imbuluzqueta, N. Guillou, C. Serre, S. R. Miller, E. Elkaim, P. Horcajada, M. J. Blanco-Prieto, *CrystEngComm* **2015**, *17*, 456-462.

[13] W. Uhl, H. R. Bock, A. Hepp, F. Rogel, M. Voss, *Z. Anorg. Allg. Chem.* **2010**, *636*, 1255-1262.

[14] a) U. Friederich, B. Fischer, J. Luthy, D. Hann, C. Schlatter, F. E. Wurgler, *Z. Lebensm. Unters. For.* **1986**, *183*, 85-89; b) P. C. Ulrich, A. Cerami, WO9202216, **1992**

[15] a) https://www.novartisoncology.com/; b) D. R. Rao, R. N. Kankan, S. Naik, M. Prabhu, IN2011MU00425A, **2013**; c) V. J. Rao, K. Mukkanti, N. A. Vekariya, P. B. Gupta, A. Islam, *Synth. Commun.* **2012**, *42*, 3200-3210.

[16] a) G. Dong, P. Ke-liang, D. Chun-ying, H. Cheng, M. Qing-jin, *Inorg. Chem.* **2002**, *41*, 5978-5985; b) U. Kumar, J. Thomas, N. Thirupathi, *Inorg. Chem.* **2010**, *49*, 62-72.

[17] T. J. Norberg-King, National Effluent Toxicity Assessment Center (NETAC) Technical Report, USEPA, **1993**, pp. 3-93.

[18] S. H. Zhang, C. S. Ye, H. R. Lin, L. Lv, X. Yu, *Environ. Sci. Technol.* **2015**, *49*, 1721-1728.

[19] a) F. M. Aarestrup, H. Hasman, *Vet. Microbiol.* **2004**, *100*, 83-89; b) L. M. Cavaco, H. Hasman, F. M. Aarestrup, *Vet. Microbiol.* **2011**, *150*, 344-348.

[20] a) J. Hrenovic, J. Milenkovic, T. Ivankovic, N. Rajic, *J. Hazard. Mater.* **2012**, *201*, 260-264; b) B. D. Corbin, E. H. Seeley, A. Raab, J. Feldmann, M. R. Miller, V. J. Torres, K. L. Anderson, B. M. Dattilo, P. M. Dunman, R. Gerads, R. M. Caprioli, W. Nacken, W. J. Chazin, E. P. Skaar, *Science* **2008**, *319*, 962-965.

[21] C. A. McDevitt, A. D. Ogunniyi, E. Valkov, M. C. Lawrence, B. Kobe, A. G. McEwan, J. C. Paton, *PLoS Pathog.* **2011**, *7*.

[22] D. Chudobova, S. Dostalova, B. Ruttkay-Nedecky, R. Guran, M. A. M. Rodrigo, K. Tmejova, S. Krizkova, O. Zitka, V. Adam, R. Kizek, *Microbiol. Res.* **2015**, *170*, 147-156.

[23] G. Porcheron, A. Garenaux, J. Proulx, M. Sabri, C. M. Dozois, *Front. Cell. Infect. Microbiol.* **2013**, *3*, 90-90.

[24] R. H. Blessing, *Acta Crystallogr., Sect. A: Found. Crystallogr.* **1995**, *A51*, 33-38.

[25] L. J. Farrugia, *J. Appl. Crystallogr.* **1999**, *32*, 837-838.

[26] G. M. Sheldrick, *Acta Crystallogr., Sect. C: Cryst. Struct. Commun.* **2015**, *71*, 3-8.

[27] S. Ahrland, R. G. Herman, *Anal. Chem.* **1975**, *47*, 2422-2426.

Supplementary Material

I. PHYSICAL DATA.

General procedure. IR spectra were recorded from KBr pellets in the range 4000-400 cm^{-1} on a PerkinElmer FT-IR Spectrometer Frontier. Thermogravimetric and differential thermal analysis (TGA-DTA) was performed using a SDT Q600 from TA Instruments equipment. Powder X-ray diffraction (PXRD) patterns were measured with a Bruker D8 diffractometer, with step size = 0.02º and exposure time = 0.5 s/step. PXRD measurements were used to check the purity of the obtained microcrystalline product by a comparison of the experimental results with the simulated patterns obtained from single-crystal X-ray diffraction data.

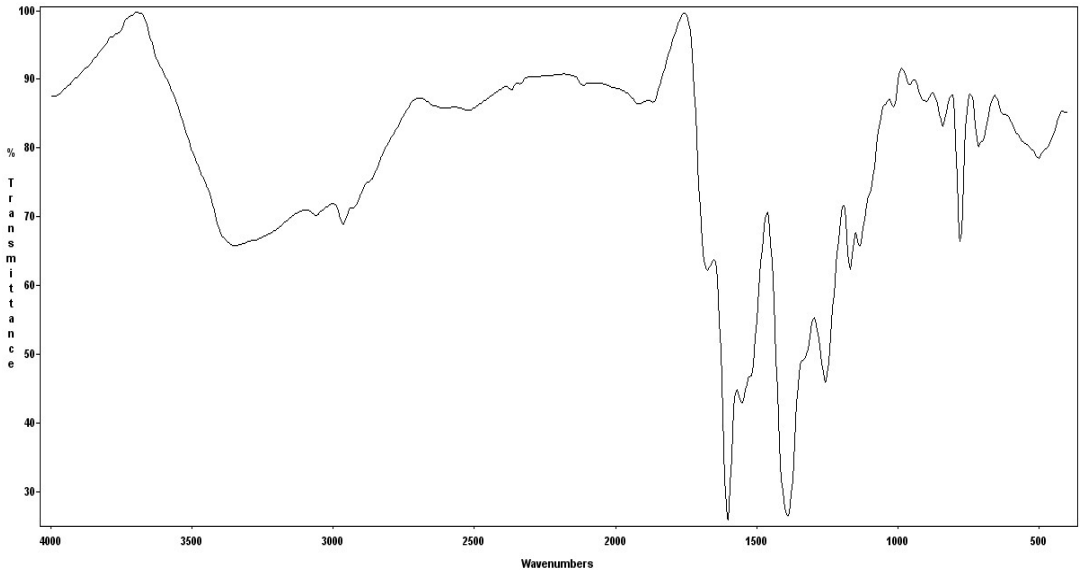

Figure S1. IR spectra in KBr for $\{[Zn(\mu\text{-}4\text{-}hzba)_2]_2 \cdot 4(H_2O)\}_n$ (**1**)

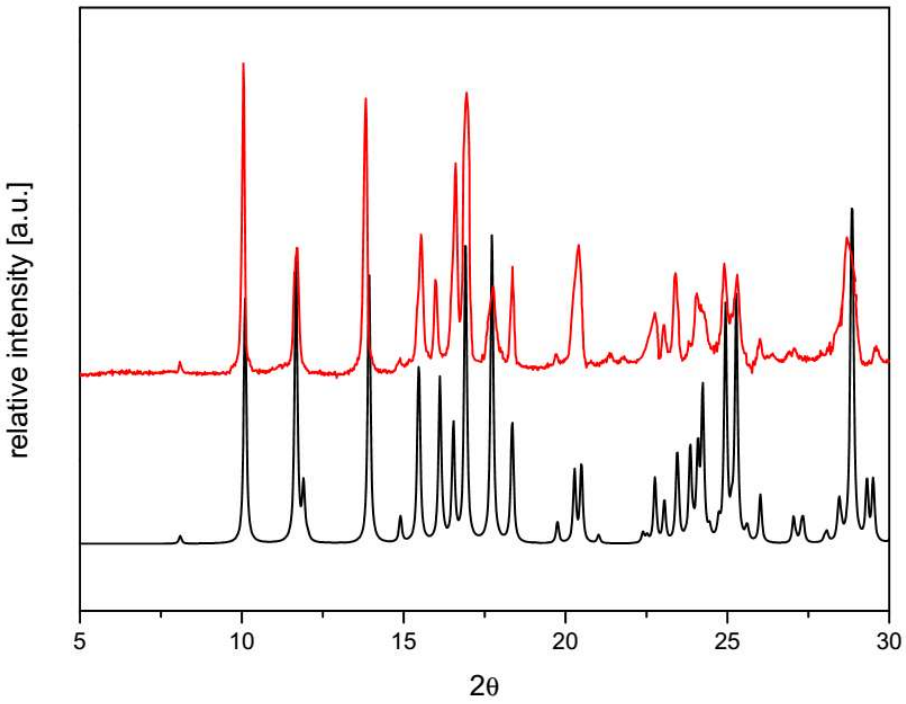

Figure S2. PDRX data for $\{[Zn(\mu\text{-}4\text{-}hzba)_2]_2 \cdot 4(H_2O)\}_n$ (**1**). Top: Experimental. Bottom: Simulated

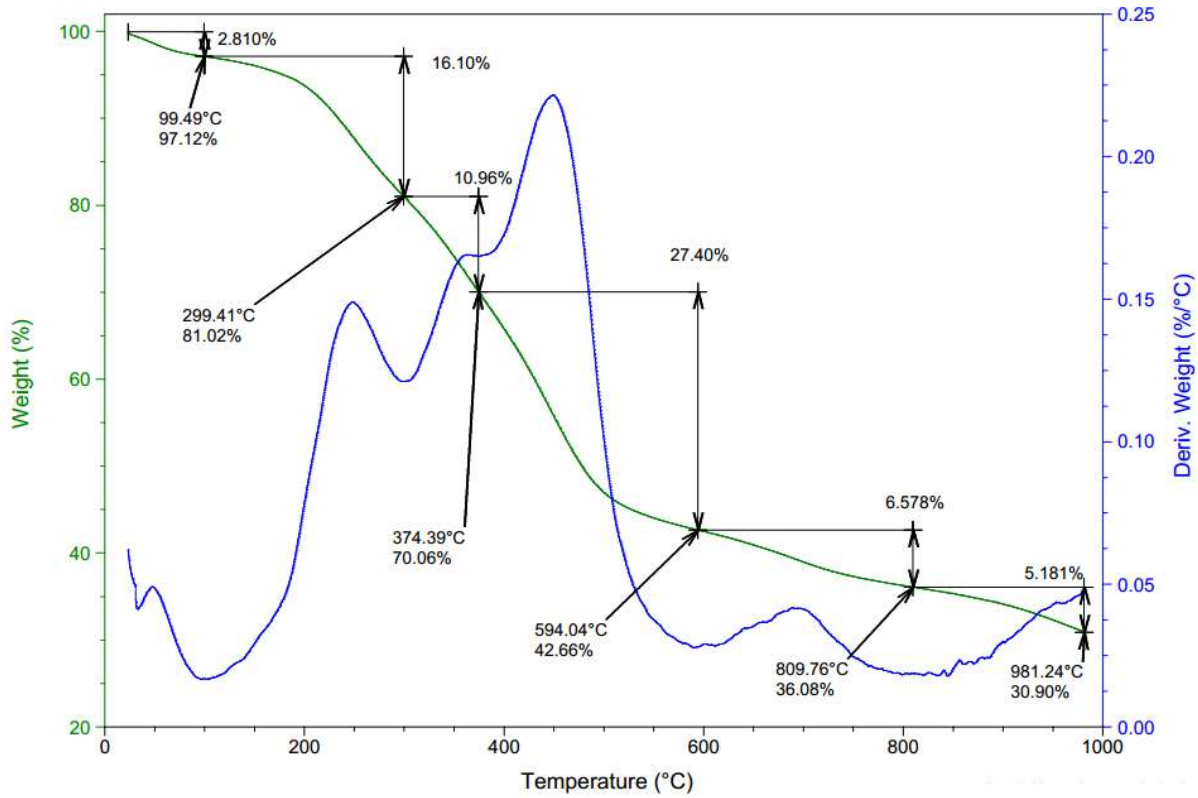

Figure S3. Thermal analysis for $\{[Zn(\mu\text{-}4\text{-}hzba)_2]_2 \cdot 4(H_2O)\}_n$ (**1**)

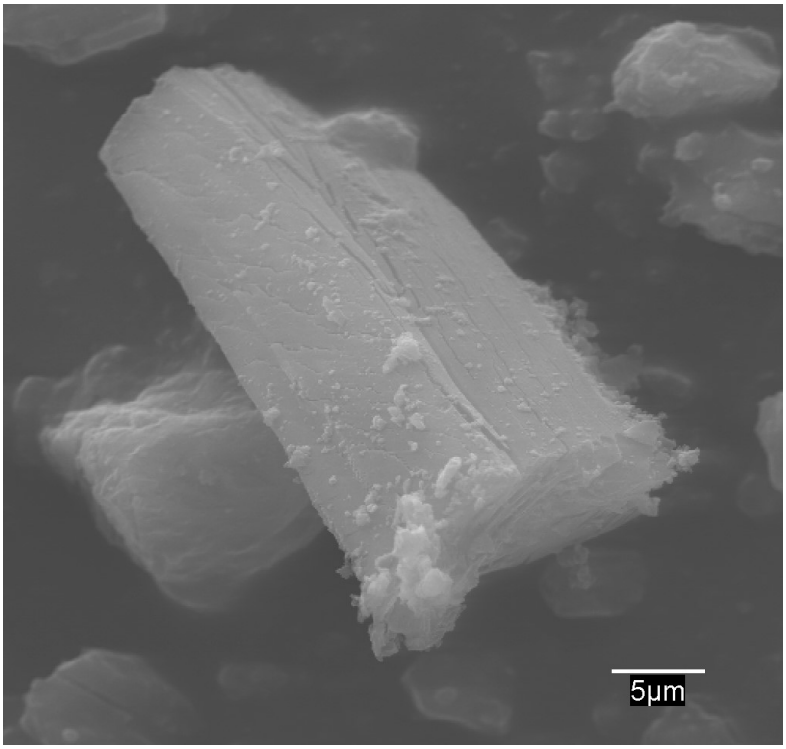

Figure S4. SEM picture for $\{[Zn(\mu\text{-}4\text{-}hzba)_2]_2 \cdot 4(H_2O)\}_n$ (**1**)

II. CRYSTAL STRUCTURE OF $\{[Zn(\mu\text{-}4\text{-}hzba)_2]_2 \cdot 4(H_2O)\}_n$ 1

Table S1. Crystallographic Data for **1**

Empirical formula	$C_{28}H_{28}N_8O_{12}Zn_2$	Z	1
Formula weight	799.35	$\rho_{calcd.}$ (g cm^{-3})	1.726
Crystal system	Triclinic	Crystal size (mm)	0.22 x 0.15 x 0.11
Space group	*1*	μ (mm^{-1})	1.639
a (Å)	7.954(15)	F_{000}	408
b (Å)	8.874(10)	λ (Å)	0.71073
c (Å)	11.604(12)	Reflns. collected	8061
α (deg.)	80.45(9)	Indep. Reflns./Rint	4941/0.07
β (deg.)	72.23(12)	GOF on F^2	1.157
γ (deg.)	87.21(13)	R_1/wR_2 ($I > 2\sigma(I)$) [a]	0.0732/ 0.2022
V (Å^3)	769.2(18)	R_1/wR_2 (all data)	0.0969/0.2116
		$\Delta\rho$ min and max (e$^-$ Å^{-3})	1.478 / -0.608

$R_1 = \Sigma(||F_o| - |F_c||)/\Sigma|F_o|$; $wR_2 = \{\Sigma[w(F_o^2 - F_c^2)^2]/\Sigma[w(F_o^2)^2]\}^{1/2}$; GOF = $\{\Sigma[w(F_o^2 - F_c^2)^2]/(n - p)\}^{1/2}$

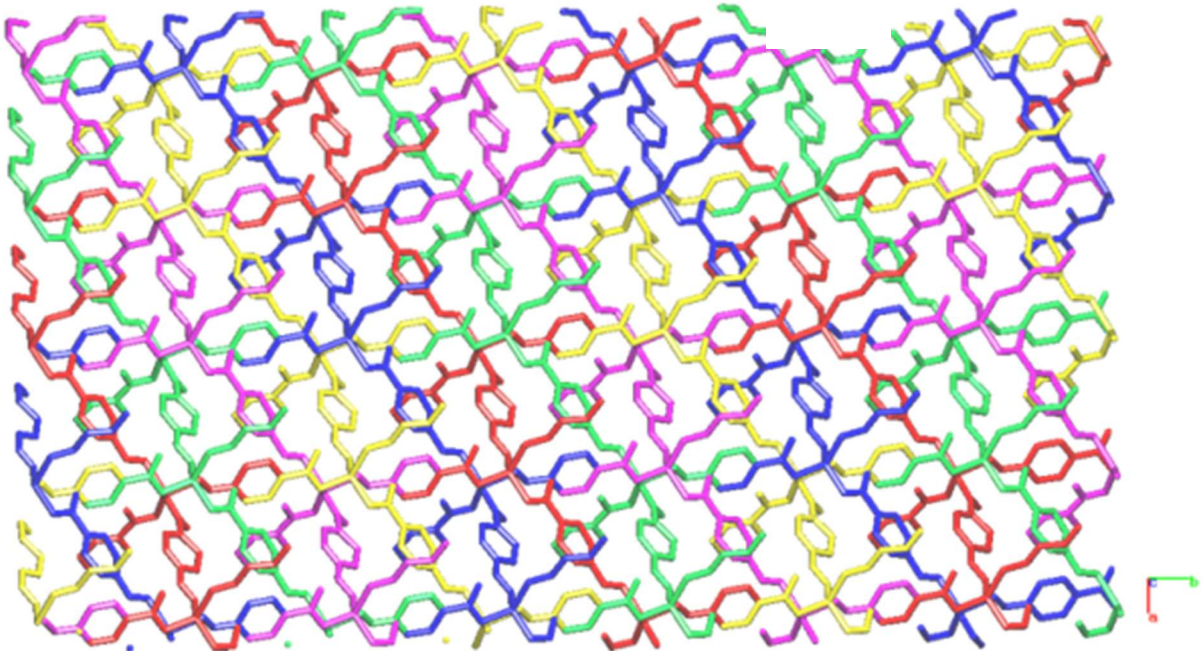

Figure S5. 3D network $\{[Zn(\mu\text{-}4\text{-}hzba)_2]_2 \cdot 4(H_2O)\}$ along *c*. Hydrogen atoms and non-coordinated water have been omitted for clarity.

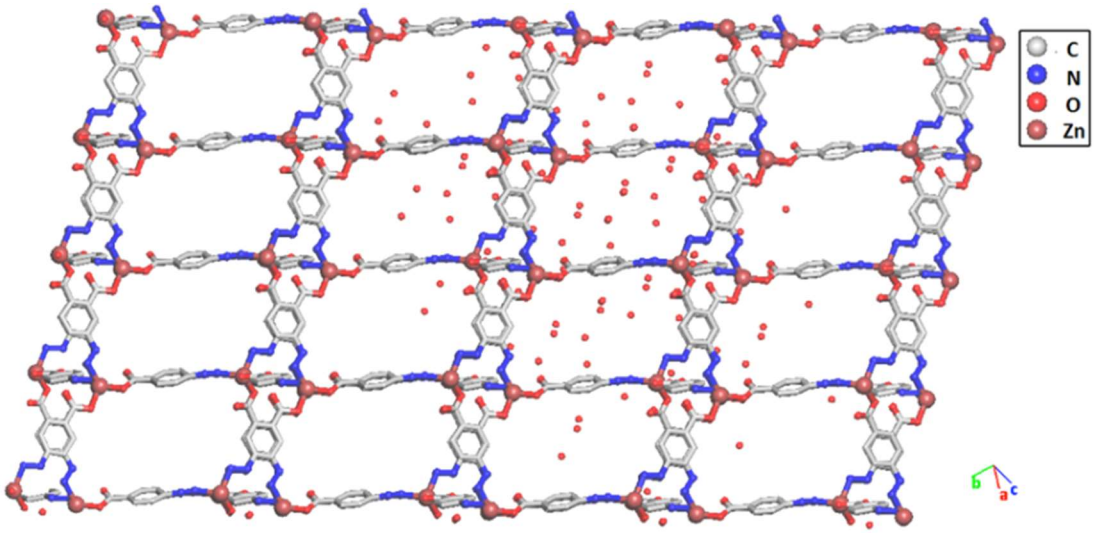

Figure S6. One of the five 3D networks that form {[Zn(μ-4-hzba)$_2$]$_2$·4(H_2O)} view along *c*. Hydrogen atoms have been omitted for clarity.

III. Microbiological assays

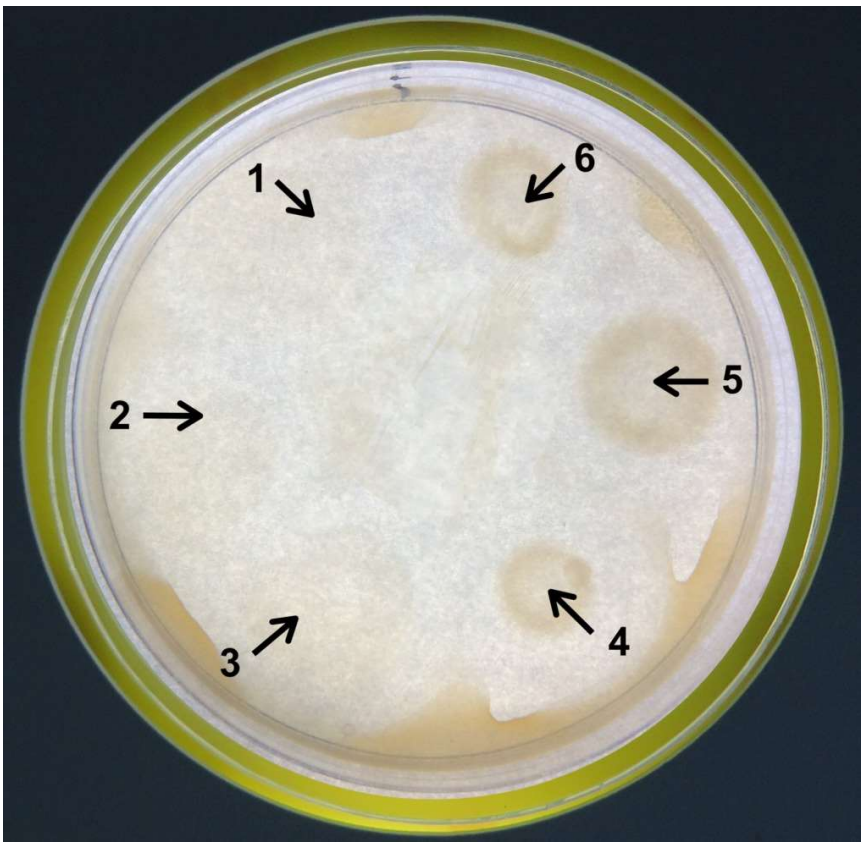

Figure S7. Inhibition assays performed by placing 1 mg approx. of each material in agar plates previously inoculated with 200 μL of *S. Aureus* suspension with 5·10^7 CFU·mL^{-1}. The plate was incubated at 36°C for 24 h. The result shows that no growth inhibition at all is produced when disposing zinc nitrate (1, 2 and 3), while for zinc acetate (4, 5 and 6) an annulus with higher bacterial density was observed, which is most probably due to the stimulatory effect of low zinc concentrations visible here as a consequence of the lower water solubility of zinc acetate in comparison with zinc nitrate.

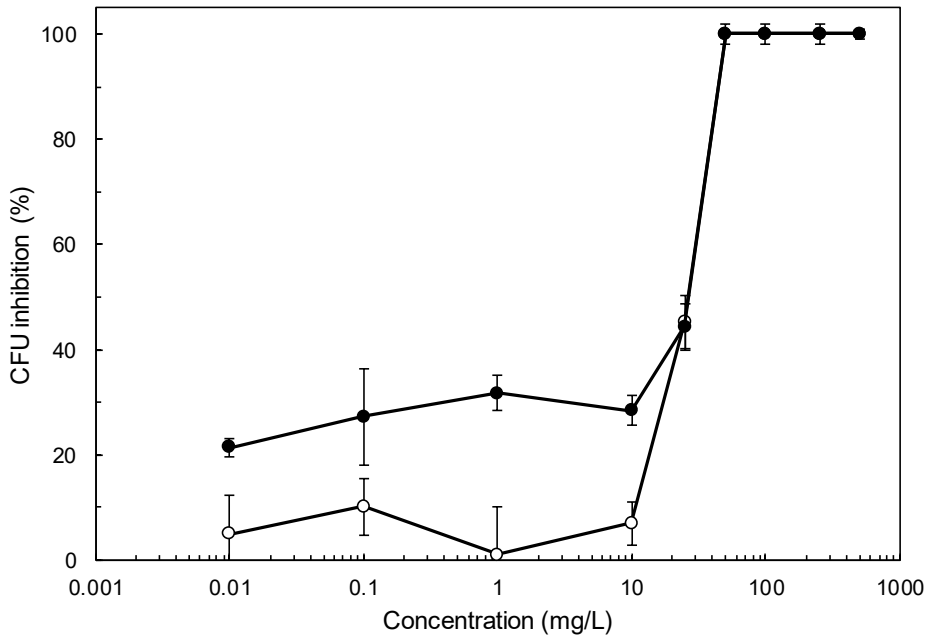

Figure S8. Colony forming unites (CFU) inhibition of *S. aureus* cells in contact with {[Zn(μ-4-hzba)$_2$]$_2$·4(H_2O)}$_n$ (filled dots) and the ligand (empty dots).

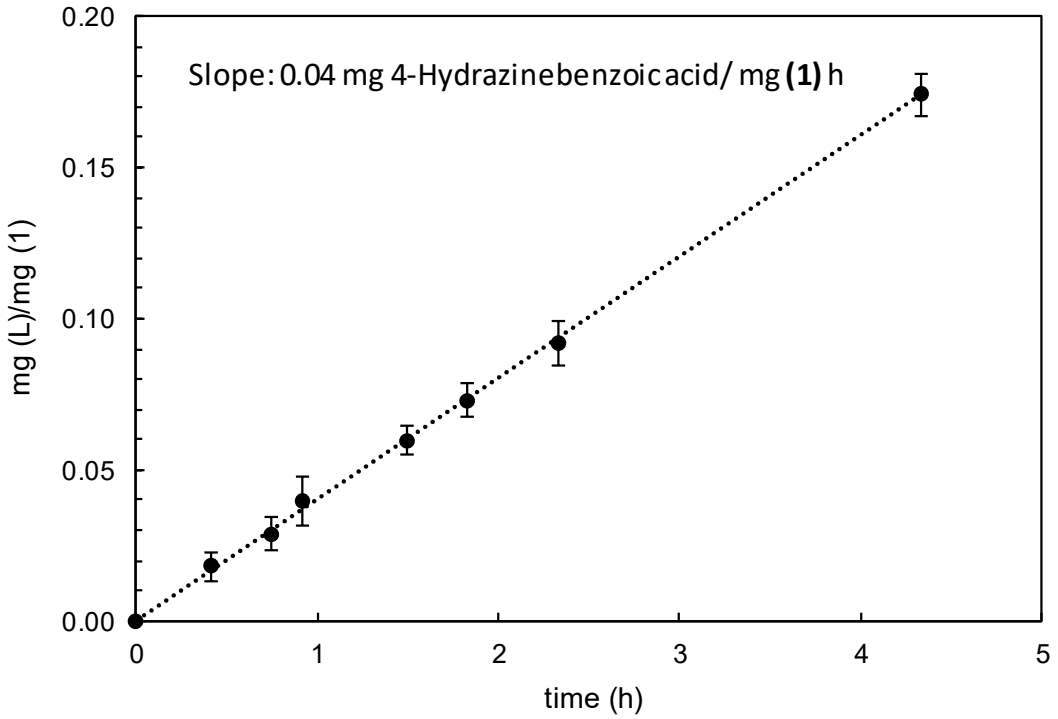

Figure S9. Solubility of the ligand in water.